

# The effect of upwelling and downwelling on turbulent entrainment in a surface stress-driven flow

Vamsi K Chalamalla

September 30, 2012

## 1 Introduction

Turbulent entrainment and mixing is an important phenomenon in many geophysical flows. The study that we consider here is relevant to the deepening of the oceanic mixed layer due to the turbulent motions created and sustained by various external processes such as wind, convection due to surface cooling and heating, breaking waves and tides. Ekman transport is a phenomenon observed in the ocean [1], where the balance between the drag due to the surface winds and the coriolis force results in a net transport  $90^\circ$  to the direction of wind. The direction of transport i.e towards the coast or away from the coast depends on the direction of wind and the direction of coriolis force. Coastal upwelling occurs when Ekman transport moves surface waters away from the coast. Surface waters are replaced by cooler and denser water from below. Similarly when Ekman transport moves surface waters towards the coast, water piles up near the coast and sinks resulting in downwelling.

The primary objective of this experimental study is to understand the effect of upwelling and downwelling on the shear driven turbulent entrainment. We consider an idealized study, with a two-layer fluid of different initial densities forced by a rotating disc . There has been many studies in the past exploring the turbulent entrainment and mixing process due to some external forcing in the absence of upwelling/downwelling. The most relevant to the present study are Shrivastava *et al.*[2], Boyer *et al.*[3] and Davies *et al.* [4]. [3] studied the evolution of a mixed layer in a two-layered fluid forced by a rotating disc at the bottom of a cylindrical tank. The basic assumption made in this study is that the rate of work done at the interface is proportional to the rate of increase of potential energy of the system. Another core assumption made in [3] is that the characteristic velocity in the mixed layer remains constant, leading to a conclusion that the depth of the mixed layer increases with time. A primarily experimental study of evolution of two-layer stratified fluid in a cylindrical tank forced at the surface by a horizontal rotating disc has been considered in [2]. They proposed two-theoretical models

1. Constant-velocity ‘V’ model, based on the assumption made by [3]
2. Constant power ‘P’ model , based on the energetics of the system.

The experimental observations from this study are compared with both the theoretical models and concluded that the rate of increase of mixed layer depth decrease with time, which

is in variance with the assumptions made in [3] .

The theoretical models proposed in [2] are taken as reference to compare our experimental results in the present study. A detailed discussion of these theoretical models will be taken up in subsequent sections below. The experimental setup is discussed in section 2 followed by observations in section 3 and finally the concluding remarks in section 4.

## 2 Experimental setup

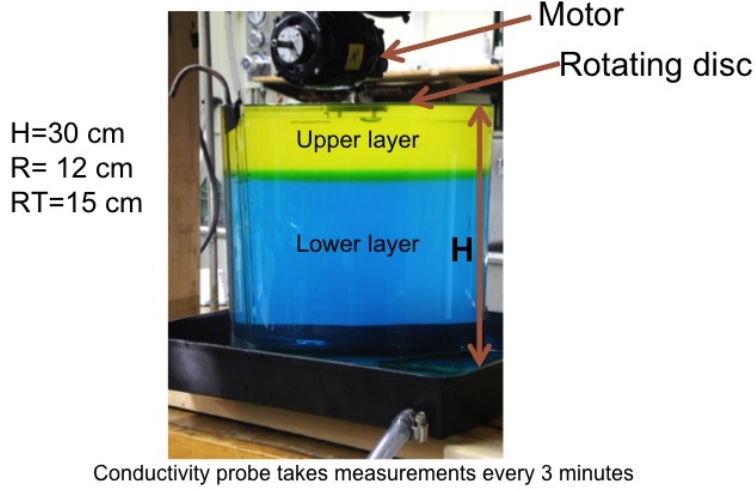


Figure 1: Experimental setup: Cylindrical tank with radius  $R_T = 15$  cm and rotating disc of radius  $R = 12$  cm.

Figure 1 shows the experimental setup. It has a cylindrical tank of radius 15 cm and a circular disc of radius 12 cm. The total height of the tank  $H$  is 30 cm. The tank is filled with two layers of fluid with densities  $\rho_{U0}$  (upper layer) and  $\rho_L$  (lower layer) with  $\rho_L > \rho_{U0}$ . The initial density difference between the two layers  $\rho_L - \rho_{U0} = \Delta\rho_0 \ll \rho_L$  so that the Boussinesq approximation is valid. The initial depth of the upper layer is denoted by  $h_0$ . The conductivity probe moves up and down within the thin gap between the rotating disc and the edge of the cylinder. The probe moves down by 33 cm from its initial position stopping at 1 cm above the bottom of the tank. The conductivity probe takes a total of 3300 measurements with 100 measurements per each cm, moving vertically with a speed of 5 mm/s. Conductivity measurements are taken only during the downward movement of the probe to avoid contamination of the data by the wake created due to the motion of the probe. The probe takes approximately 1 minute for the downward pass and 1 minute for the upward return pass to the initial position and the wait time between each pass is slightly less than 1 minute. So, the conductivity profiles are available with an interval of 3 minutes at every point in the path of the probe. Density is computed based on these conductivity measurements. The rotating disc is controlled by a motor, shown in figure 1. The vertical position of the disc is adjusted before the experiment such that it is just below the surface of upper layer. The lower and upper layer fluids are dyed with different colors to visualize

the interface between the two layers. All the fluids used in the experiment were stored for couple of days before the experiment to ensure that there is no temperature difference between the fluids, which may result in unnecessary convective motions. To calibrate the probe, the conductivity of upper layer, the lower layer and an equal mixture of lower and upper layer fluids has been measured before and after the experiment. There is little drift in the probe measurements for the experiments which lasted for shorter duration ( 2 hours). For experiments which lasted more than 3 hours, there is some considerable drift in the probe measurements and the profiles has been corrected keeping the lower layer density constant (i.e  $\rho_L$  measured at a later time has been corrected to match with the  $\rho_L$  measured at  $t=0$ ). The disc starts rotating as soon as the conductivity probe starts its second profile. Since it takes some time for the rotating disc to spin up the upper layer, we define the zero time for our experiments as 3 minutes after the disc starts rotating. Three different scenarios has been considered in our experiments. Firstly, a standard no-flux experiment with no upwelling or downwelling is considered i.e  $Q_B = 0$ . The second scenario is the upwelling experiment. Denser fluid is pumped into the tank using a micropump at a volumetric rate  $Q_B > 0$  from bottom of the tank. As fluid starts filling up from below, it pushes up the entire fluid in the tank with an average upward velocity given by  $Q_B/A$ , where  $A$  is the cross-section of the tank given by  $\pi R_T^2$ . The excess water in the tank overflows from above, which is collected into a tray in which the cylindrical tank is placed as shown in the schematic of the experiment. The third scenario is the downwelling experiment, where the lower layer (denser) fluid is sucked out the tank at a rate  $Q_B < 0$  by reversing the direction of the micropump. Simultaneously, fluid of density  $\rho_{U0}$  is pumped into the upper layer at the same rate, resulting in a downward velocity ( $Q_B/A$ ) for the entire volume of the fluid.

### 3 Experimental results

Table 1 shows the list of different experiments done in our present study. The parameters which are varied in this study are initial density difference between two layers  $\Delta\rho_0$ , rotation rate of the disc  $\Omega$  and the initial upper layer depth  $h_0$ . A positive value of  $Q_B$  represents an upwelling experiment and negative values of  $Q_B$  represents downwelling experiments. When  $Q_B = 0$ , there is no upwelling or downwelling, we refer to this experiment as no-flux experiment in the following sections.

We observe that the rotating disc at the surface sets the upper layer into turbulent motion, since the Reynolds number in the flow defined by  $Re = UR/\nu \equiv \Omega R^2/\nu$  is of the order of 20,000. We do not measure fluid velocities in our experiments, so we do not have quantitative details of the velocity field in the upper layer. But, from previous studies and also the direct observation by looking at the experiment, there is an evidence of large scale circulation in the upper layer as shown schematically in figure 2. There is a mean flow in the upper layer with velocities in the azimuthal and radial directions apart from the turbulent velocities. Fluid particles near the surface are pushed away towards the walls, due to the rotation of the disc. Also, shadowgraph images (which we discuss in more detail below) shows that there is a dome-like structure near the center of the tank at the interface, showing the upward motion of denser fluid as discussed in [3] and [2]. So the fluid particles which are pushed towards the walls at the center come down along the wall, setting up a

<i>Experiment</i>	$Q_B(cc/s)$	$\Delta\rho_0(g/cc)$	$\Omega rad/s$	$h_0(cm)$	$H(cm)$	Symbol
$DL\Delta\rho_{01}\Omega 2h_{01}$	-0.59	0.01782	2	10	30	$\triangle$
$DH\Delta\rho_{02}\Omega 2h_{01}$	-1.18	0.02382	2	10	30	+
$DL\Delta\rho_{02}\Omega 2h_{01}$	-0.59	0.02382	2	10	30	+
$DL\Delta\rho_{02}\Omega 3h_{01}$	-0.59	0.02382	3	10	30	+
$N\Delta\rho_{02}\Omega 2h_{01}$	0	0.02382	2	10	30	+
$N\Delta\rho_{03}\Omega 2h_{01}$	0	0.03782	2	10	30	$\circ$
$N\Delta\rho_{04}\Omega 2h_{01}$	0	0.05082	2	10	30	$\square$
$N\Delta\rho_{03}\Omega 3h_{01}$	0	0.03782	3	10	30	$\circ$
$N\Delta\rho_{02}\Omega 2h_{02}$	0	0.02382	2	13.5	27	+
$UL\Delta\rho_{01}\Omega 2h_{01}$	0.59	0.01782	2	10	30	$\triangle$
$UL\Delta\rho_{02}\Omega 2h_{01}$	0.59	0.02382	2	10	30	+
$UL\Delta\rho_{04}\Omega 2h_{01}$	0.59	0.05082	2	10	30	$\square$
$UL\Delta\rho_{03}\Omega 2h_{01}$	0.59	0.03782	2	10	30	$\circ$
$UL\Delta\rho_{04}\Omega 3h_{01}$	0.59	0.05082	3	10	30	$\square$
$UL\Delta\rho_{02}\Omega 2h_{03}$	0.59	0.02382	2	15	30	+
$UH\Delta\rho_{02}\Omega 2h_{01}$	1.18	0.02382	2	10	30	+
$UH\Delta\rho_{04}\Omega 2h_{01}$	1.18	0.05082	2	10	30	$\square$
$UH\Delta\rho_{03}\Omega 2h_{01}$	1.18	0.03782	2	10	30	$\circ$

Table 1: Dimensional parameters of the experiments.

return circulation.

The turbulent motions in the upper layer ensure that the fluid in the upper layer is well mixed. As time progresses, the density difference between the two layers decreases as the denser fluid in the lower layer is lifted up against gravity and mixed into the upper layer. Meanwhile, the upper mixed layer grows deeper with time, with a sharp interface between the two layers. All these turbulent motions and the circulation are confined to the upper layer, while the lower layer remains quiescent during the experiment, since the density jump across the interface suppresses the fluid motion to be penetrated into the lower layer. We show the characteristic thickness of the interface  $d_I$  in figure 2. The variation in the interfacial thickness is observed to be very little between different experiments, so it is assumed to be a constant in our calculations. An important non-dimensional parameter in this study is the bulk Richardson number given by

$$Ri_B = \frac{g'_U h_U}{\Omega^2 R^2}, \quad (1)$$

where  $h_U$  is the depth of the upper layer,  $g'_U = g(1 - \bar{\rho}_U/\rho_L)$  is the reduced gravity of the upper layer. Another non-dimensional parameter which is relevant to this study is the interfacial Richardson number defined as,

$$Ri_I = \frac{g'_U d_I}{u_U^2} \equiv \frac{g'_U h_U}{u_U^2} d_I, \quad (2)$$

where  $u_U$  is the characteristic velocity of the upper layer.

The bulk Richardson number  $Ri_B$  is a measure of balance between the strength of overall stratification and the external forcing. While the interfacial Richardson number  $Ri_I$  represents the balance between a local measure of stratification and shear across the interface. We are particularly interested in how the entrainment depends on the local and bulk parameters of the flow. We define layer richardson number for the mixed layer  $Ri_L$  as

$$Ri_L = \frac{g'_U h_U}{u_U^2}, \quad (3)$$

which is based on the mixed (upper) layer depth and the characteristic velocity of the upper layer.

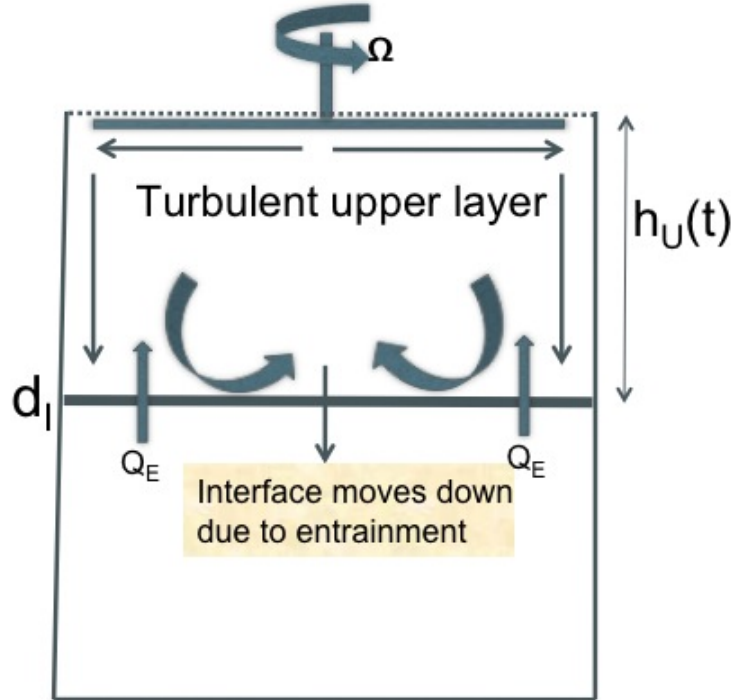


Figure 2: Schematic showing the flow in the upper mixed layer

The blue solid line in the figure 3 shows a typical density profile from the experiment. Normalized density  $\hat{\rho}$  is plotted against depth,

$$\hat{\rho} = \frac{\rho - \rho_{U0}}{\rho_L - \rho_{U0}}, \quad (4)$$

Where  $\rho_{U0}$  is the initial upper layer density and  $\rho_L$  is the density of lower layer, which doesn't change during the experiment. The average of the upper layer and lower layer

densities is calculated and the depth corresponding to the averaged density is considered as the upper(mixed) layer measured from the surface. The red dot shown in the figure represents this interface location. An important assumption made to calculate the interface depth is that the density in the lower layer, i.e below the interface is  $\rho_L$ . Actually, it is not exactly true as evident from the density profile (solid line). Due to the secondary mixed layer (as discussed in more detail by [6]) formed just below the interface the average density of the lower layer is slightly below  $\rho_L$ , which results in some error which can be quantified from the experimental and the theoretical density profiles.

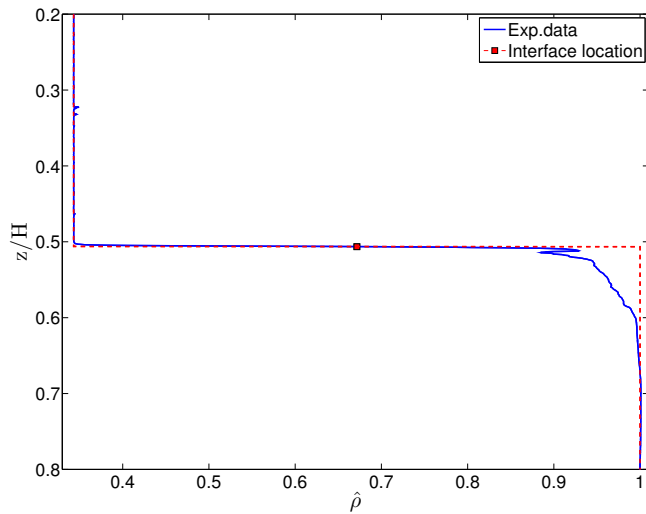


Figure 3: Figure showing the typical density profile from the experimental data. The red dot represents the interface density which is obtained by averaging the density of the upper layer  $\rho_U$  and lower layer  $\rho_L$

### 3.1 Previous theoretical models

As discussed in the introduction of this report, two models were proposed by [2] to study the evolution of mixed layer in a initial two-layered fluid forced by a rotating disc at the surface of mixed layer. The power supplied at the interface in terms of the interfacial stress is given by

$$\mathcal{P} = \pi R^2 c_D \rho_L u_U^3, \quad (5)$$

where  $c_D$  is an empirically determined drag coefficient,  $u_U$  is the characteristic-velocity of the upper mixed layer and  $R$  is the radius of the disc.

The potential energy of the system defined in [2] is given by,

$$\mathbb{P}\mathbb{E} = \pi R^2 \left( -g \int_0^{h_U} \rho_U z dz - g \int_{h_U}^H \rho_L z dz + \frac{g \rho_L H^2}{2} \right) \equiv \pi R^2 \rho_L \frac{g'_{U} h_U^2}{2} \quad (6)$$

According to the assumption that,  $\frac{d}{dt}\mathbb{P}\mathbb{E} \propto \mathcal{P}$ , we obtain

$$\frac{d}{dt}h_U \propto \frac{u_U^3}{g'_U h_U}, \quad (7)$$

Defining  $\frac{d}{dt}h_U$  as the entrainment velocity  $u_E$  as discussed in [2]. It is important to remember that [2] discussed no-flux experiments i.e when  $Q_B = 0$ . More generalized formula for the entrainment velocity will be defined in the later section.

$$u_E \propto \frac{u_U^3}{g'_U h_U}. \quad (8)$$

Now defining the entrainment parameter as  $u_E/u_U$ , the entrainment parameter scales with richardson number as

$$\frac{u_E}{u_U} \propto \frac{1}{Ri_L}. \quad (9)$$

From the above equation , the entrainment parameter scales with the inverse of Richardson number for no-flux experiments. In the subsequent sections, we will try to fit our experimental data with this scaling, to check if the data for upwelling and downwelling experiments agrees with it.

To compare the experimental data with the theoretical models, a rescaled time variable was defined in [2] as

$$\tau_* = \frac{R}{h_0} \frac{c_V}{Ri_B} \tau, \quad (10)$$

where  $\tau$  is the non-dimensional time given by  $\tau = \Omega t$ ,  $c_V$  is an empirically determined constant.

V-model is based on the assumption made by [3], that the characteristic velocity in the upper layer remains constant and it scales with the velocity induced by the rotating disc which  $R\Omega$ . Based on these arguments, the non-dimensional mixed layer depth  $\hat{h}_U = h_U/h_0$  varies with  $\tau_*$  as

$$\hat{h}_U = 1 + \tau_* \quad (11)$$

However, P-model proposed by [2] argue that the constant power input from the rotating disc cannot maintain a constant velocity in the upper layer considering the energetics of the system. They propose that, as the mixed layer deepens more volume of fluid needs to be energized continuously by the rotating disc. The power input from the disc should be balanced by a rate of increase of kinetic energy, the viscous dissipation and the power required to mix the fluid. If a constant velocity in the mixed layer is assumed, then the kinetic energy of the upper layer (discussed in more detail by [2]) given by

$$\mathbb{K}\mathbb{E} = \frac{1}{2}\rho_L\pi R^2 h_U u_U^2, \quad (12)$$

increases continuously, so the dissipation of kinetic energy also increases. This is not possible to maintain with a constant power input from the disc, leading to an assumption that the kinetic energy of the upper layer remains constant. Using this assumption, the time evolution of the mixed layer depth  $\hat{h}_U$  is given by,

$$\hat{h}_U = (1 + 5\tau_*/2)^{2/5} \quad (13)$$

Figure 4 shows the evolution of interface depth for one of the no-flux experiments with  $\Delta\rho = 0.03782g/cc$  and  $\Omega = 2s^{-1}$ ,  $h_0 = 10$  cm. The non-dimensional depth  $\hat{h}_U = h_U/h_0$  is plotted against  $\tau_*$ . The black line represents the *P model*, the red line represents the experimental data and the blue line represents the *V model*. Initially, the non-dimensional mixed layer depth increases linearly with time. Since for small  $\tau_*$ , the P-model reduces to V-model (by neglecting the higher order terms in the expansion), it is difficult to distinguish between P-model and V-model during the initial times. But as time progresses the rate of increase of mixed layer depth is not constant but clearly decreases following the *P model*.

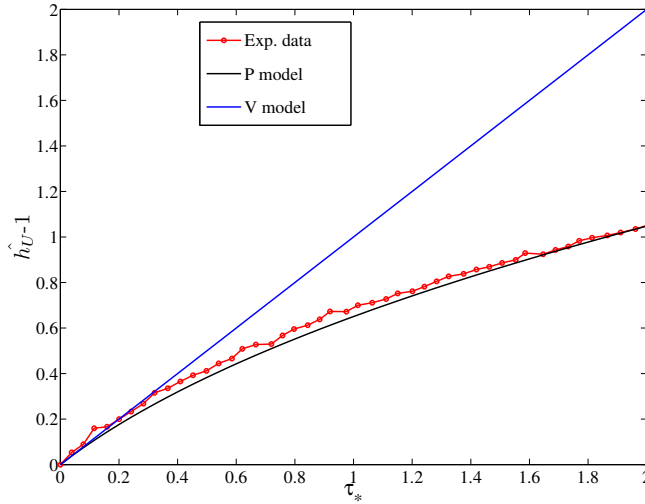


Figure 4: Time evolution of upper layer depth:  $\hat{h}_U$  plotted against  $\tau_*$ . Comparison of experimental data with the theoretical models.

### 3.2 Equations for upwelling experiment ( $Q_B > 0$ )

In general, the equation for the rate of mass change in the cylinder is given by,

$$\pi R_T^2 \frac{d}{dt} \left( \bar{\rho}_U h_U + \rho_L (H - h_U) \right) = \rho_L Q_B - \bar{\rho}_U Q_B \quad (14)$$

$$\implies \pi R_T^2 \frac{d}{dt} \left( g \left( \frac{\rho_L - \bar{\rho}_U}{\rho_L} \right) h_U \right) = -g \left( \frac{\rho_L - \bar{\rho}_U}{\rho_L} \right) Q_B \quad (15)$$

$$\implies \pi R_T^2 \frac{d(g'_U h_U)}{dt} = -g'_U Q_B. \quad (16)$$

The equation for the rate of volume change of the upper layer is given by,

$$\pi R_T^2 \frac{dh_U}{dt} = Q_E - Q_B \quad (17)$$

where  $Q_E$  is the volumetric entrainment rate across the interface.

Substituting (17) into (16), we obtain an expression for volumetric entrainment rate across the interface  $Q_E$ , given by

$$Q_E = -\pi R_T^2 h_U \frac{1}{g'_U} \frac{dg'_U}{dt} \equiv \pi R_T^2 \frac{dh_U}{dt} + Q_B \quad (18)$$

Now, generalizing the definition of entrainment velocity  $u_E$  as the volumetric entrainment flux  $Q_E$  divided by the cross-section area of the tank,

$$u_E = \frac{dh_U}{dt} + Q_B/(\pi R_T^2). \quad (19)$$

It is important to note that this definition of the entrainment velocity is valid for no-flux ( $Q_B = 0$ ), upwelling ( $Q_B > 0$ ) and downwelling ( $Q_B < 0$ ) experiments.

### 3.3 Equations for downwelling experiment ( $Q_B < 0$ )

The equation for the rate of mass change in the cylinder is given as,

$$\pi R_T^2 \frac{d}{dt} \left( \bar{\rho}_U h_U + \rho_L (H - h_U) \right) = \rho_L Q_B - \bar{\rho}_{U0} Q_B \quad (20)$$

$$\implies \pi R_T^2 \frac{d}{dt} \left( g \left( \frac{\rho_L - \bar{\rho}_U}{\rho_L} \right) h_U \right) = -g \left( \frac{\rho_L - \bar{\rho}_{U0}}{\rho_L} \right) Q_B \quad (21)$$

$$\implies \pi R_T^2 \frac{d(g'_U h_U)}{dt} = -g'_{U0} Q_B. \quad (22)$$

As already noted by [2], for no-flux experiments where  $Q_B = 0$ ,  $g'_U h_U$  remains constant (mass conservation) i.e the bulk richardson number defined in (1) remains constant. However for upwelling and downwelling experiments mass is not conserved since we are adding external fluid into the tank, and so the bulk Richardson number  $Ri_B$  changes during the experiment thus giving us a scope to study the entrainment process over a range of Richardson numbers by performing a single experiment. Specifically, for upwelling experiments since  $Q_B > 0$ ,  $g'_U h_U$  decreases and so the bulk Richardson number  $Ri_B$  decreases whereas for downwelling experiments,  $Ri_B$  increases during the experiment.

It is important to note that for downwelling experiments, fresh water of density  $\rho_{U0}$  is added continuously from the top. Mathematical representation of this addition is given by the second term on the R.H.S of (20). Whereas in upwelling experiments the volume of fluid flowing out of the tank has density  $\rho_U$  (density of the mixed upper layer), as evident from the second term in R.H.S of (14).

Substituting (17) into (22), we obtain the expression for volumetric entrainment rate across the interface  $Q_E$ , given by

$$Q_E = Q_B \left( 1 - \frac{g'_{U0}}{g'_U} \right) - \pi R_T^2 h_U \frac{1}{g'_U} \frac{dg'_U}{dt} \equiv \pi R_T^2 \frac{dh_U}{dt} + Q_B \quad (23)$$

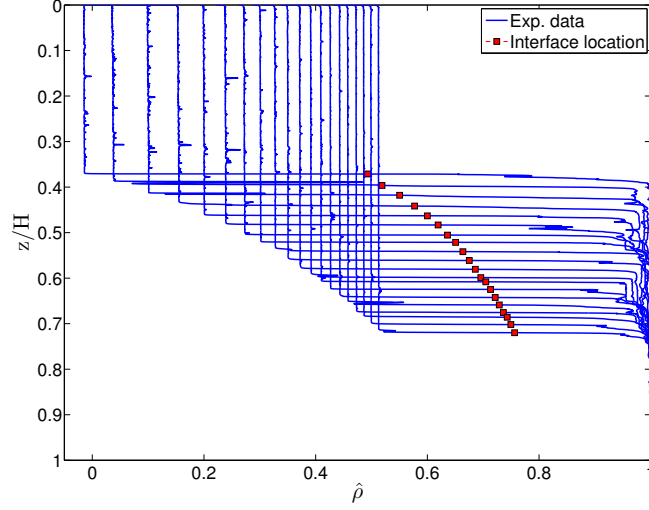


Figure 5: Plots of  $\hat{\rho}$  against  $z/H$  for an experiment with  $\Omega = 2 \text{ rad s}^{-1}$ ,  $\Delta\rho = 0.02382\text{g/cc}$ ,  $Q_B = 0$  Starting with  $t=0$ , profiles are shown with a time interval of 9 minutes. Experiment  $N\Delta\rho_0\Omega^2h_{01}$  shown in table 1

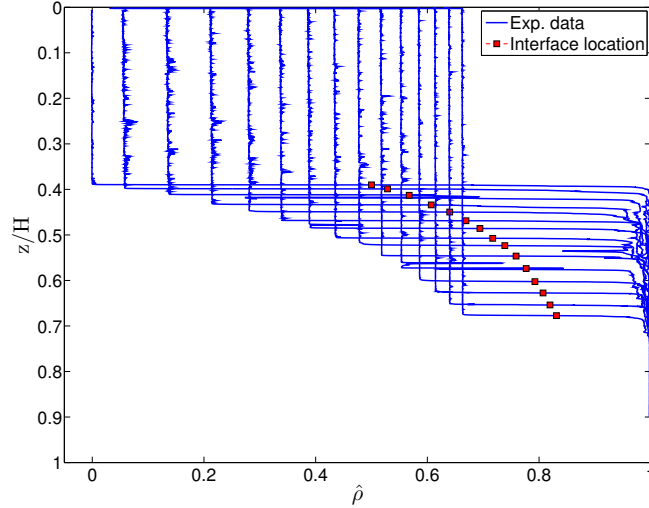


Figure 6: Plots of  $\hat{\rho}$  against  $z/H$  for an experiment with  $\Omega = 2 \text{ rad s}^{-1}$ ,  $\Delta\rho = 0.02382\text{g/cc}$ ,  $Q_B = 0.59 \text{ cc/s}$ . Starting with  $t=0$ , profiles are shown with a time interval of 9 minutes. Experiment  $UL\Delta\rho_0\Omega^2h_{01}$  shown in table 1

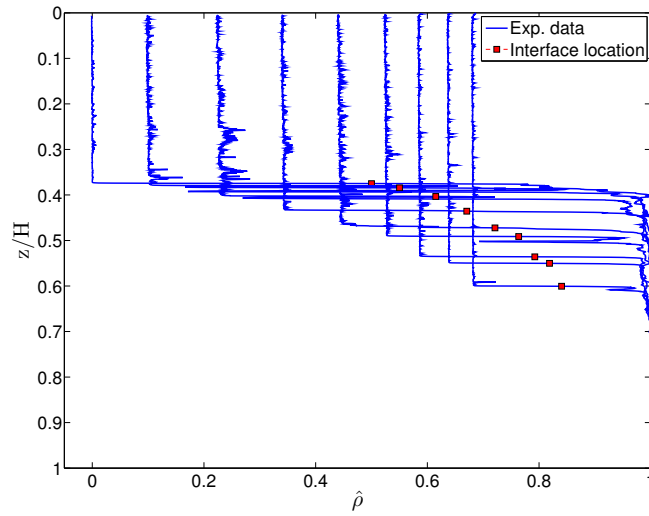


Figure 7: Plots of  $\hat{\rho}$  against  $z/H$  for an experiment with  $\Omega = 2 \text{ rad s}^{-1}$ ,  $\Delta\rho = 0.02382\text{g/cc}$ ,  $Q=1.18 \text{ cc/s}$ . Starting with  $t=0$ , profiles are shown with a time interval of 9 minutes. Experiment  $UH\Delta\rho_{02}\Omega 2h_{01}$  shown in table 1

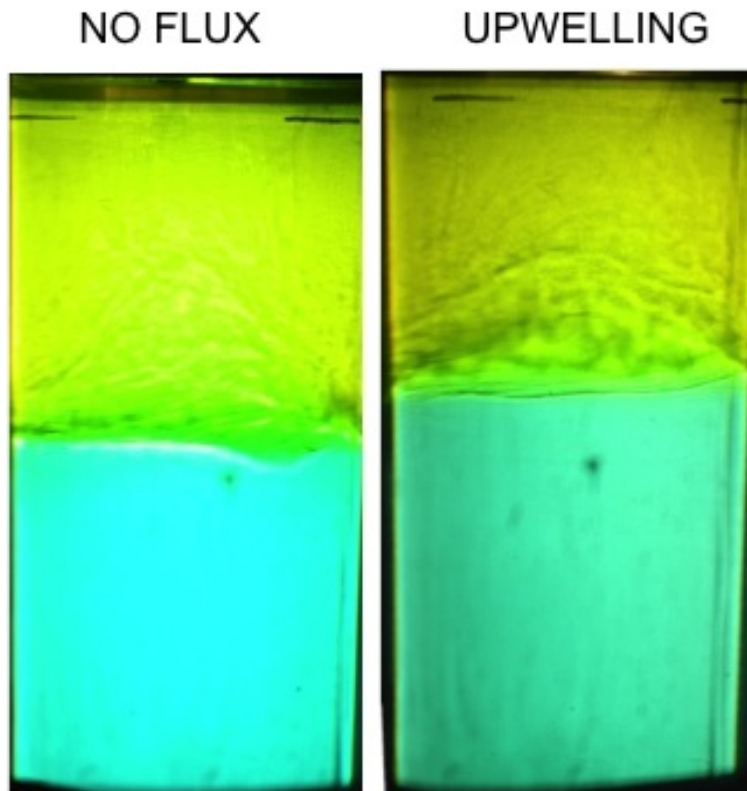


Figure 8: Shadowgraph images of the upwelling and no-flux experiments at a particular time.

Figure 5 shows plots of normalized density profiles of a no-flux experiment with  $\Omega = 2 \text{ rad s}^{-1}$ ,  $\Delta\rho = 0.02382\text{g/cc}$ ,  $Q_B = 0$ . Density profiles are shown at different time instances starting with  $t=0$  (3 minutes from the time disc started rotating). Time goes from left to right in this figure i.e the left most profile is time  $t=0$ . The time interval between each profile is 9 minutes ( every 3 profiles). Red square shaped dots shown in the figure represent the location of interface. As time progresses, the interface moves down, and the density difference between the two layers decreases.

There are four important things to note here,

1. The interface between the two layers is sharp, similar to ‘scouring’ observed by Woods *et al.* (2000) [5],
2. the upper layer is well homogenized (mixed),
3. The interface depth is clearly not varying linearly with time,
4. A secondary relatively thin mixed layer is observed just below the interface, with the density closer to the lower layer density.

Overtuning is observed near the interface at certain times indicating a possibility of Kelvin-Helmholtz instability at the interface. Figure 6 shows density profiles for an upwelling experiment with  $Q_B = 0.59\text{cc/s}$ . The important qualitative difference between the no-flux and upwelling experiment profiles is that the magnitude of density fluctuations in the mixed layer seems to be higher in the upwelling experiment and also the density overturnings at the interface seems to be more frequent in the upwelling experiment. Similarly, figure 7 shows density profiles for an upwelling experiment with  $Q_B = 1.18\text{cc/s}$ . The density fluctuations seems to be even higher and also the density overturnings are more frequent and intense. Also, the density difference between the two layers is dropping quickly in the case of upwelling experiments compared to the no-flux experiment. Quantitative discussion of these differences will be discussed in the sections below. Figure 8 show the shadowgraph images of the upwelling and no-flux experiments at a particular time instant. Though the images are not very clear, it is apparent that there is more turbulent activity in the upper layer of upwelling experiment, confirming the qualitative differences observed in the density profiles.

Similar comparison between the no-flux and upwelling experiments for different density differences ( $\Delta\rho = 0.03782, 0.05082\text{g/cc}$ ) show the identical qualitative differences observed above, suggesting that this phenomenon is a feature of any upwelling flow irrespective of the range of Richardson numbers. However, there will be quantitative differences in the entrainment rate and the rate of increase of mixed layer depth as the density difference get higher, due to the fact that the entrainment becomes difficult as the stratification grows stronger. A detailed quantitative analysis is required to determine whether this phenomenon is observed independent of the Richardson number. Quantitative comparison of density variance and the entrainment rate is discussed in detail in the following sections.

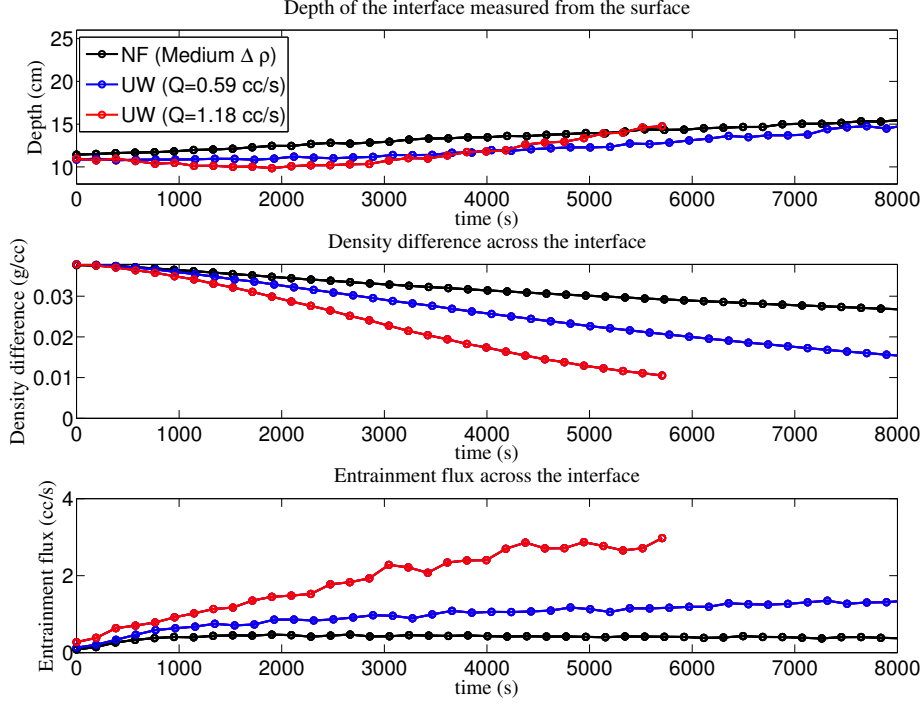


Figure 9: Plots showing the quantitative comparison of no-flux and upwelling experiments  $\Omega = 2 \text{ rad s}^{-1}$ ,  $\Delta\rho = 0.03782\text{g/cc}$ ,  $Q_B = (0, 0, 59, 1.18) \text{ cc/s}$ . (a) Time evolution of upper layer depth (b) Time evolution of density difference between the upper and lower layer. (c) Time evolution of volumetric entrainment flux  $Q_E$  across the interface as defined in (18).

Figure 9 is shown here to explain the quantitative differences between the no-flux and upwelling experiments. Figure 9(a) shows the interface depth plotted against time. Figure 9(b) shows the density difference between the two layers plotted against time and finally figure 9(c) shows the volumetric entrainment rate (defined in (18) ) plotted against time. The black line represents the no-flux experiment. Red and blue lines represent upwelling experiments with different upwelling rates  $Q_B$ . Initially, the rate at which the depth of the mixed layer increases is slower for upwelling experiments when compared with the no-flux experiment. This is due to the fact that  $Q_B > 0$  for upwelling experiments and from equation (17), since  $Q_B$  appears with a negative sign on the R.H.S of the evolution equation for mixed layer depth, it decreases the growth rate of mixed layer depth. When  $Q_B = 1.18 \text{ cc/s}$ , i.e when the upwelling rate is higher, the initial evolution of mixed layer depth shows that  $\frac{dh_U}{dt} < 0$  because the upwelling rate  $Q_B$  dominates the volumetric entrainment flux  $Q_E$  across the interface. But, at a later time, the entrainment flux increases and is higher in upwelling experiments when compared with the no-flux experiment as shown in figure 9(c). As a result, the rate of increase of mixed layer depth is higher for upwelling experiments when compared with the no-flux experiment, as evident from the later time evolution shown in figure 9(a).

Another important quantitative difference to note between the upwelling and no-flux experiment is the rate at which the density difference between two layers drops. For upwelling experiments, the rate of decrease of density difference is higher and it increases with  $Q_B$ . This can be attributed to the higher entrainment rate in the upwelling experiments, because more entrainment occurs when the density difference across the interface is relatively weak.

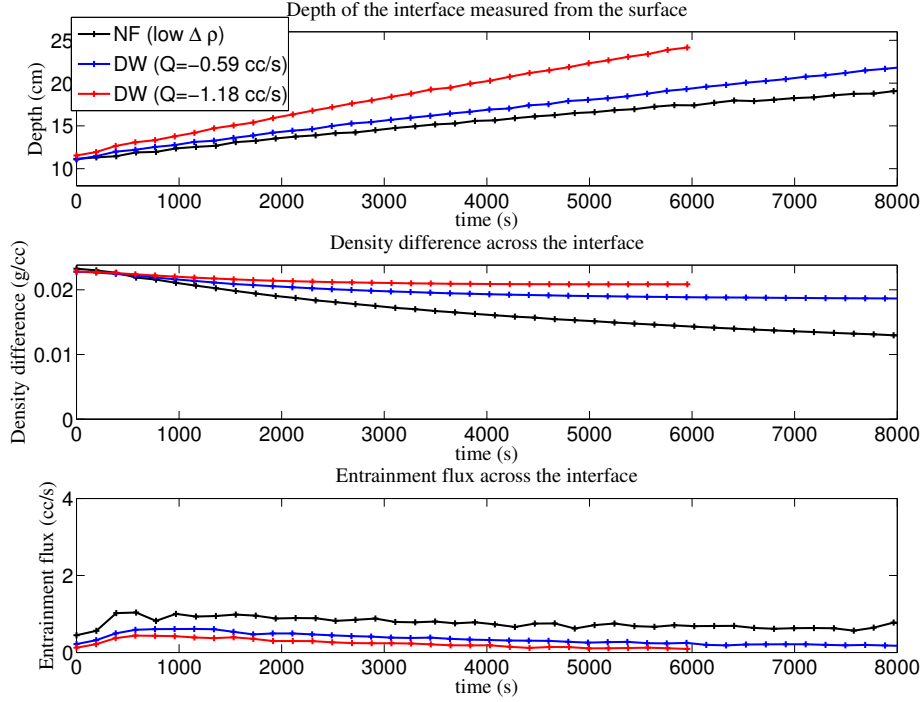


Figure 10: Plots showing the quantitative comparison of no-flux and downwelling experiments  $\Omega = 2 \text{ rad s}^{-1}$ ,  $\Delta \rho = 0.02382 \text{ g/cc}$ ,  $Q_B = (0, -0, 59, -1.18) \text{ cc/s}$ . (a) Time evolution of upper layer depth (b) Time evolution of density difference between the upper and lower layer. (c) Time evolution of volumetric entrainment flux  $Q_E$  across the interface as defined in (23).

Figure 10 is shown here to explain the quantitative differences between the no-flux and downwelling experiments. Figure 10(a) shows the interface depth plotted against time, figure 10(b) shows the density difference between the two layers plotted against time and finally figure 10(c) shows the volumetric entrainment rate (defined in equation 11) plotted against time. The black line represents the no-flux experiment. Red and blue lines represent downwelling experiments with different  $Q_B$ . Here, the time evolution of mixed layer depth shows that the higher the value of  $Q_B$ , higher the rate of increase of mixed layer depth as evident from figure 10(a). Since  $Q_B < 0$  for downwelling experiments, from equation (17), it is evident that this term increases the rate of increase of mixed layer depth. Figure 10(b) shows that the rate at which the density difference between two layers drops is slower compared to the upwelling experiments shown in figure 9(b). Also, the volumetric entrainment rate shown in figure 10(c), suggest a reverse trend as compared to the upwelling experi-

ments i.e higher the downwelling rate, lower the volumetric entrainment flux  $Q_E$ . However, difference between volumetric entrainment rates of no-flux and downwelling experiments is not as significant as observed in the upwelling experiments. The quantitative analysis of upwelling and downwelling entrainment rates will be discussed in detail in the subsequent sections.

Figure 11 shows the time averaged density variance in a semi log plot plotted against  $Q_B$ . Time averaged density variance is given by,

$$\text{Time averaged density variance } \langle \langle \rho'^2 \rangle_z \rangle_t = \frac{1}{T} \frac{1}{(h_U - 2)} \int_{t=0}^T \int_1^{h_U-1} [\rho'(z, t)]^2 \quad (24)$$

where  $\rho'(z, t) = \rho(z, t) - \bar{\rho}_U(z)$  is the fluctuating component of the density field,  $\bar{\rho}_U(z)$  represents the time average density of the upper (mixed) layer.  $T$  is the duration of the experiment. Spatial averaging is done in the upper layer, starting at a depth 1 cm below the surface and stopping at 1 cm above the interface. 'Δ' symbol represents the lowest  $\Delta\rho$  considered in our experiments which is 0.01782 g/cc, '+' symbol represents  $\Delta\rho = 0.02382$  g/cc, 'o' represents  $\Delta\rho = 0.03782$  g/cc and '□' represents the highest density difference which is 0.05082 g/cc. Black and grey color represents no-flux experiments, red and magenta represents downwelling experiments, blue and cyan represent upwelling experiments. As discussed in the previous sections, turbulent fluctuations appear to be higher in the upwelling experiments. The density variance plot shown here quantify the turbulent fluctuations. Clearly, there seems to be a trend in the density variance when plotted against  $Q_B$ . It is important to remember that  $Q_B > 0$  represents upwelling experiments,  $Q_B < 0$  represents downwelling experiments and  $Q_B = 0$  represents no-flux experiments. As  $Q_B$  goes from negative to positive values, in general the density variance increases significantly. Clearly, the density variance is highest for upwelling experiments with higher  $Q_B$ , which suggests that the turbulent fluctuations increase with increasing upwelling rate. However there are two exceptions in the figure with red colored 'Δ' and magenta colored '+'. High density variance is observed in these experiments because of the fact the initial density difference is low in these experiments (see table 1) and also the rotation rate is higher in one of these experiments (magenta colored '+').

The reason for higher turbulent fluctuations in upwelling experiments can be explained using the reynolds stress terms. For example, considering a fluid particle in an upwelling experiment. The fluid particle which is below the interface, due to the vertical velocity induced by the upwelling is moving from static flow field into a turbulent (mixed layer) flow field. As a result, the fluid particle tends to resist the motion resulting in negative  $u'$  (fluctuating horizontal velocity), which makes the product  $-u'w' > 0$ , increasing the reynolds stresses. Evolution equation for turbulent kinetic energy is given by

$$\frac{d(TKE)}{dt} = P - \epsilon + B - \frac{\partial T'_i}{\partial x_j} \quad (25)$$

where  $P$  is the turbulent production term given by  $-\langle u'w' \rangle \frac{d\bar{U}}{dz}$ . Since the mean flow gradi-

ent  $\frac{d\bar{U}}{dz} > 0$  the turbulent production term is positive, thus increasing the turbulent kinetic energy.

Now considering the evolution equation for density variance

$$\frac{d(\langle \rho'^2 \rangle)}{dt} = P_\rho - \epsilon_\rho - \frac{\partial T'_{\rho i}}{\partial x_j} \quad (26)$$

where  $P_\rho$  is the scalar production term given by  $-\langle \rho' w' \rangle \frac{d\bar{\rho}}{dz}$ . Since the mean density gradient across the interface  $\frac{d\bar{\rho}}{dz} < 0$ , fluctuating vertical velocity  $w' > 0$  (discussed above) and the density fluctuation  $\rho'$  is observed to be positive, the scalar production term is positive, contributing to the increase in density variance.

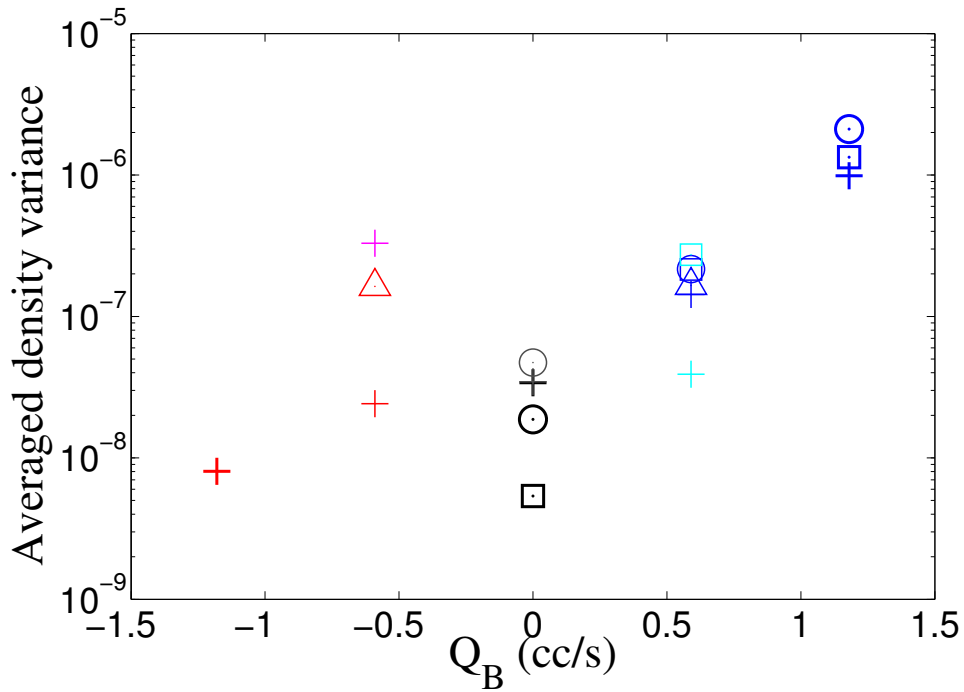


Figure 11: Plot showing the time-averaged density variance for all the experiments.

Figure 12 shows the entrainment parameter defined in (9) plotted against  $\tau_*$ . Thick solid blue colored lines represent upwelling experiments with  $Q_B = 1.18$  cc/s, thin blue/cyan colored lines represent upwelling experiments with  $Q_B = 0.59$  cc/s. Red/magenta colored lines represent downwelling experiments. Black/grey colored lines represent no-flux experiments. For all the downwelling and no-flux experiments, the entrainment parameter increases and reaches almost a steady value at a later time. For upwelling experiments with  $Q_B = 0.59$  cc/s, the entrainment parameter increases initially and appears to reach a steady value at a later time which is greater than the time taken for no-flux experiments. However at  $Q_B = 1.18$  cc/s, the time span for which we have the experimental data, the entrainment hasn't reached a steady value. Another important thing to notice in this figure is that,

for all the downwelling and no-flux experiments, the entrainment parameter appears to be reaching an approximately same steady value irrespective of the initial density difference. Similarly, for upwelling experiments with  $Q_B = 0.59$  cc/s, the entrainment parameter seems to be reaching a steady value of approximately 1. For all upwelling experiments with  $Q_B = 1.18$  cc/s, the entrainment parameter seems to be reaching a steady value of approximately  $2 \times 10^{-4}$ , which is double the steady value for  $Q_B = 0.59$  cc/s. This suggests that, the entrainment parameter may scale with the upwelling rate  $Q_B$ , irrespective of the initial density difference. However, due to the large scatter in the data presented in this figure, it is difficult to come to a conclusion regarding the scaling of entrainment parameter with  $Q_B$ .

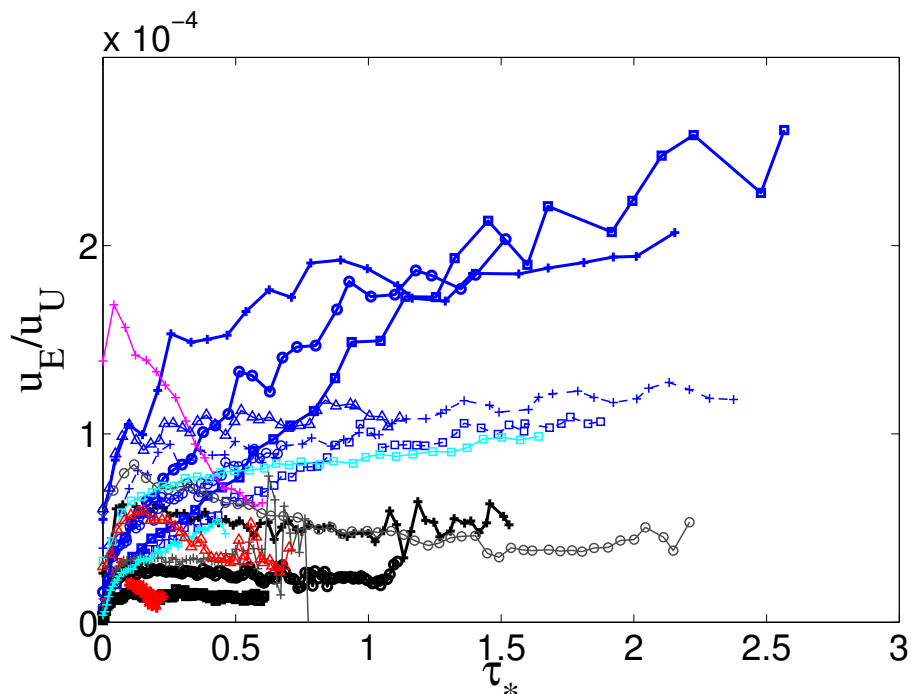


Figure 12: Plots of entrainment parameter plotted against  $\tau^*$  for all the experiments.

Figure 13 shows the entrainment parameter for all the downwelling and no-flux experiments plotted against  $1/Ri_L$  which is defined as

$$1/Ri_L = \frac{u_U^2}{g'_U h_U} \equiv \frac{u_U^2 h_U}{g'_U h_U^2} \propto \frac{\text{KE}}{\text{PE}}, \quad (27)$$

For no-flux experiments, since the denser fluid is continuously lifted up and mixed, the potential energy is expected to increase. Also for downwelling experiments, lighter fluid is added at a greater height and heavier fluid which is at lower height is taken out and also there is entrainment process where the work is done to lift the heavy parcel up. The net change in potential energy of the system during this process is observed to be positive resulting in an increase of potential energy of the system for downwelling and no-flux

experiments. So from figure 13, since x-axis represent the ratio of kinetic energy to the potential energy, time goes from right to left. The experimental data shown in figure 13 seems to fit well with the black solid straight line shown in the same figure, suggesting that the scaling law derived above is valid i.e entrainment parameter is proportional to  $1/Ri_L$ . So, the entrainment dynamics is dependent on the bulk parameters of flow rather than the local flow dynamics.

In upwelling experiments, the heavier fluid is added into the tank at a lower height (which increases potential energy), where as the mixed layer fluid overflows out of the tank at a greater height (which reduces potential energy), and also there is an increase in potential energy due to the turbulent entrainment. The net change in potential energy observed in upwelling experiments is negative, thus reducing the potential energy of the system. Figure 14 shows the data from upwelling experiments plotted along with the no-flux and downwelling experiments. For upwelling experiments, since the potential energy of the system is observed to decrease, time goes from left to right in figure 14, whereas the time goes from right to left for all downwelling and no-flux experiments. It is evident from the figure that the entrainment parameter for the upwelling experiments does not obey the same scaling as the downwelling and no-flux experiments, since there is clear deviation as the time progresses. The reason for this deviation from the standard scaling is probably due to the fact the turbulent fluctuations in the upwelling experiments are higher , resulting in different entrainment and interfacial dynamics.

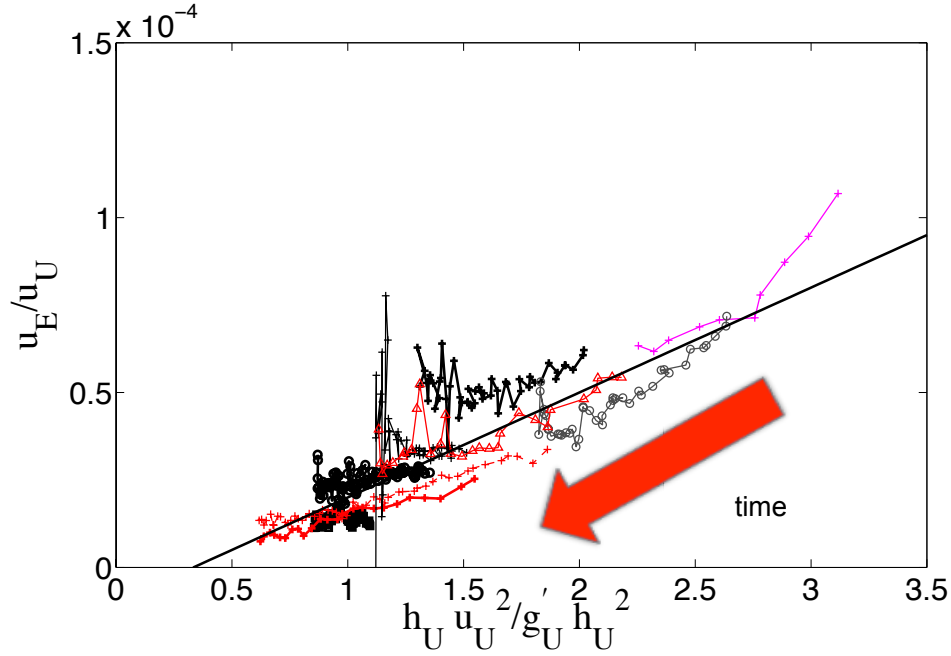


Figure 13: Plots of entrainment parameter plotted against  $1/Ri_L$  for all the downwelling and no-flux experiments.

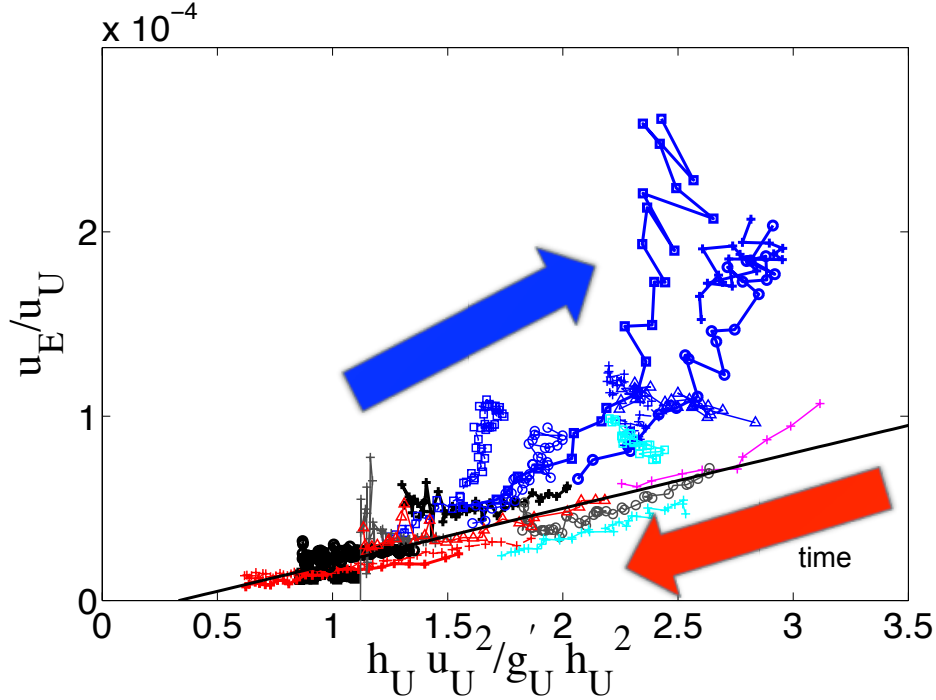


Figure 14: Plots of entrainment parameter plotted against  $1/Ri_L$  for all the experiments.

## 4 Conclusions

We have conducted an experimental study to consider the effect of upwelling and downwelling on the shear-driven turbulent entrainment. Different controlling parameters involved in this study are disc rotation rate  $\Omega$ , initial upper layer depth  $h_0$ , initial density difference  $\Delta\rho_0$ . Upwelling and downwelling experiments were performed considering two different flow rates  $Q_B = 0.59, 1.18$  cc/s. The layer Richardson number  $Ri_L$  as defined in (3) varies from 0.3 to 2. The density profiles for standard no-flux experiments shows that the mixed layer depth does not vary linearly with time, rather its rate of increase drops at later time following the P-model. Qualitative and quantitative analysis of our experimental results show that the upwelling experiments are observed to be qualitatively different with measurably enhanced turbulent fluctuations leading to new and increased entrainment rate. This increase in entrainment rate is probably due to the higher turbulent fluctuations and density variance. A clear trend is observed for time averaged density variance when plotted against  $Q_B$ , i.e density variance increases monotonically as  $Q_B$  increases. The increase in turbulent fluctuations in upwelling experiments is due to the enhanced Reynolds stresses induced by the upwelling. As explained in section 3 above, the upwelling results in the increased scalar and turbulent production terms thus increasing the turbulence and net transport across the interface. Monotonic increase in density variance with  $Q_B$  is because the vertical velocity  $w'$  increases with  $Q_B$  resulting in higher scalar production term.

The entrainment parameter  $u_E/u_U$  as defined in (9) for upwelling experiments does not

obey the standard scaling law, which states that the entrainment parameter  $u_E/u_U$  is proportional to  $1/Ri_L$ . Standard scaling suggests that the entrainment rate across the interface is dependent solely on the bulk parameters of the upper layer, rather than the interfacial Richardson number which is the measure of ratio of the local stratification strength and the velocity drop across the interface. Since, for upwelling experiments the entrainment rate is not a function of the layer Richardson number and also the density variance is dependent on the upwelling rate  $Q_B$ , more detailed analysis is needed consider the upwelling rate  $Q_B$  along with the Richardson number to come up with a scaling law.

Downwelling does not seem to influence the entrainment dynamics significantly. It is evident from the fact that the density variance is low, when compared with the no-flux experiments and also the entrainment parameter obeys the standard scaling law. Since the experiments are performed in lab (small) scale, the relevance of these experimental results in oceanic scales is not clear and needs better understanding through numerical simulations and observational studies in the ocean.

### Acknowledgements

This study was part of the Geophysical Fluid Dynamics Program at Woods Hole Oceanographic Institution. I would like to thank Colm Caulfield and Claudia Cenedese for advising me on this project . Also, I would like to thank all the GFD staff and fellows for making this program a memorable experience.

### References

- [1] Knauss, J.A., Introduction to Physical Oceanography, Waveland Press. Second Edition. 2005, c1997
- [2] Shrivastava, A., Cenedese, C. & Caulfield, C. P. 2012. Entrainment and mixing dynamics of surface-stress-driven stratified flow in a cylinder. *J. Fluid Mech.*, 691, 498-517.
- [3] Boyer, D. L., Davies, P. A. & Guo, Y. 1997. Mixing of a two-layer stratified fluid by a rotating disc. *Fluid Dyn. Res.*, 21, 381-401.
- [4] Davies, P. A., Guo, Y., Boyer, D. L. & Folkard, A. M. 1995. The flow generated by the rotation of a horizontal disk in a stratified fluid. *Fluid Dyn. Res.*, 17, 27-47.
- [5] Woods, A. W., Caulfield, C. P., Landel, J. R. & Kuesters, A. 2010. Non-invasive turbulent mixing across a density interface in a turbulent Taylor-Couette flow. *J. Fluid Mech.*, 663, 347-357.
- [6] Georgy Manucharyan , Dynamics of the mixed layers in stratified shear flows, GFD summer program 2010.